
Article:
Mitra, B., Hilden, J. and Litster, J.D. orcid.org/0000-0003-4614-3501 (2016) Compaction mechanics of plastically deformable dry granules. Powder Technology, 291. pp. 328-336. ISSN 0032-5910

https://doi.org/10.1016/j.powtec.2015.12.022

Compaction mechanics of plastically deformable dry granules

Biplob Mitra[1,2], Jon Hilden[2,3], James D Litster[1,4]

[1]Department of Industrial and Physical Pharmacy, Purdue University, West Lafayette, IN, USA

[2]Small Molecule Design and Development, Eli Lilly and Co., Indianapolis, IN, USA

[3]School of Materials Engineering, Purdue University, West Lafayette, IN, USA

[4]School of Chemical Engineering, Purdue University, West Lafayette, IN, USA

ABSTRACT:

To improve the understanding of how dry granulation and in particular, granule solid fraction (SF) impact the compaction behavior of plastically deformable microcrystalline cellulose (MCC), in this study, the Drucker Prager Cap (DPC) model parameters were calibrated using monodisperse MCC dry granules. Small cylindrical compacts of MCC with SF in the range of 0.40 to 0.70 were used as model dry granules which were monodisperse in both size and SF. Virgin MCC powder and granules were compressed into tablets with SF in the range of 0.70 to 0.90. The DPC parameters (cohesion, internal friction angle, cap eccentricity, and hydrostatic yield stress), Young's modulus and Poisson's ratio were experimentally determined from diametrical and uniaxial compression, and in-die compaction tests. Results showed that calibration of the shear failure surface only may be adequate for MCC granules when the DPC model is completely calibrated for virgin MCC. Increasing granule SF significantly decreased the cohesion only. All other parameters were impacted by the tablet SF only. In the 2D yield surface, the shear failure surface expanded as the granule SF increased. MCC of any granulation status requires the same in-die compaction stress state for densification to a given tablet solid fraction.

KEYWORDS: Deformable Dry Granules, Tablet, Solid Fraction, Tensile Strength, Drucker-Prager Cap (DPC) Model

Correspondence to:

Prof. James D Litster
Purdue University
480 Stadium Mall Drive, Room 027A
West Lafayette, IN 47907, USA
Telephone +1 765 496 2836
Fax +1 765 494 0805
Email address: jlitster@purdue.edu

1. Introduction

Granulation and tableting are common processing steps in the pharmaceutical industry. Powders are converted into granules via various granulation techniques and then forward processed into tablets of desired quality attributes such as tensile strength, content uniformity, and dissolution. Despite the much-advanced understanding of the compaction processes and the availability of state-of-the-art compaction equipment, robust production of quality tablets still remains a significant challenge to date. Problems such as low strength, chipping, lamination, or capping of tablets can occur upon scale-up [1,2]. Identifying these issues early in development will allow necessary adjustments to the composition, processes, or even to equipment and tooling to avoid or at least minimize process and product upsets at large scale.

It is difficult to develop a holistic understanding of the evolution of tablet structure as well as tableting problems using the typical empirical methods such as Heckel analysis, Kawakita equation, and Hiestand indices [3]. To accomplish this the Drucker Prager Cap (DPC) model, a phenomological model originally developed for soil mechanics, has recently been adopted in the pharmaceutical industry [4,5]. In this model, the powder aggregates are regarded as continuum medium and powder compaction is regarded as a forming event as the properties of the material evolve [5]. Commonly used material parameters such as cohesion, angle of

internal friction, and yield stress, and their dependence on tablet solid fraction (SF), are used to calibrate the model. DPC parameters are used as input in the Finite Element Model (FEM) to predict local mechanical properties evolved during the consolidation of powder in a tableting or roll compaction operation [4,5,6,7,8].

To date, DPC model parameters have been mostly reported for virgin powders, and to a limited extent, for their mixtures. Calibration of the DPC model parameters for various systems of microcrystalline cellulose (MCC) powder, such as MCC PH101 [4,9], MCC PH102 [5,9], MCC PH 200 [9], lubricated MCC PH101 [7], MCC PH102 with unlubricated die [6], a binary mixture of 90% MCC PH102 and 10% acetaminophen [9] were reported in the literature. Diarra et al. [10] reported DPC parameters of a cosmetic powder composed of talc and 5% fatty substance. In a more recent work, LaMarche et al. [11] determined DPC parameters of MCC PH102, pregelatinized starch, lactose monohydrate, lactose anhydrate, and dicalcium phosphate and evaluated tableting risk associated with each material. They also determined DPC parameters of various high shear wet granulated and roll-compacted formulations, and searched for correlation among the material properties and tableting issues (e.g., crack, sticking, capping, chipping, and low strength). However, granule properties were not adequately controlled in this study to understand their impact on the DPC parameters.

Dry granules are particle agglomerates produced under pressure. The physical changes that occur to granules during a confined compression process are important in the evolution of the tablet microstructure. Granule size, shape, and density, as well as granule-granule friction and granule-tooling surface friction could also affect the consolidation process. In our previous study, we have demonstrated that TS of tablets decreased approximately linearly as the dry granule SF increased [12]. Recently we also have demonstrated that (i) tablets formed from deformable dry granules fracture both intra-granularly and extra-granularly, (ii) the proportion of each type is dependent on the deformation potential (defined as tablet SF – initial SF of the packed granule bed), and (iii) the tablet TS is correlated to the product of intra-granular fracture and final SF of granules in the tablet [13]. In the current study, DPC parameters of monodisperse MCC granules of varying SF were determined to improve the

mechanistic understanding of the effect of dry granule SF on the compaction behavior of MCC.

2. DPC Model

A detailed description of the DPC model is available in the literature [5]. The model describes yielding of materials as a function of hydrostatic stress (p), deviatoric stress (q) and SF of the tablet. The material is considered to be isotropic. The compaction stress state is expressed by p and q. p causes densification, whereas q causes material distortion without volume change. During consolidation, the yield loci expand as the compact SF increase, which signifies a greater resistance to further plastic deformation. Figure 1 shows the 2D yield surface of the material as a limiting curve $F\ (q, p, SF) = 0$.

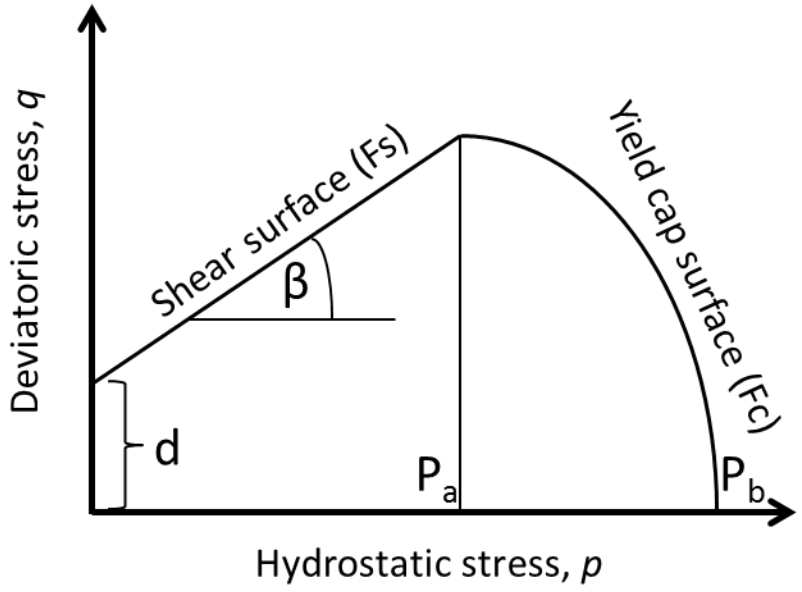

Figure 1. 2D Yield Surface for the Modified Drucker Prager/Cap Model

The model consists of two curves in the p-q plane as shown in Figure 1.

1. A shear failure (F_s) showing increasing q value with increasing p value. The shear line characterizes the shear stress in a powder necessary to cause fracture. F_s in the p-q plane is defined as:

$$F_s(q,p) = q - d - p\ tan\beta = 0 \tag{1}$$

where q is the deviatoric stress, p is the hydrostatic stress, d is the material cohesion, and β is the internal angle of friction. The intersection of Fs with the q axis represents the material cohesion (d), and the slope of the F_s line is the friction angle of material (β). The line is the boundary between the stress states that cause elastic deformation versus permanent deformation of the solid. Shear failure typically results in fracture of the structure.

2. The elliptical cap (F_c) intersects both the p and q axes. Material densifies in this region. F_c in the p-q space, is defined as:

$$F_c(q,p) = \sqrt{(p - p_a)^2 + [R \cdot q]^2} - R \cdot (d + p_a \cdot\ tan\,\beta) = 0 \tag{2}$$

where R is the cap eccentricity parameter, p_a is defined as the cap evolution parameter (the onset of volumetric plastic strain driven densification).

Complete calibration of the model requires four independent yield surface parameters, which are d, β, R, and p_b (hydrostatic yield strength). d is a measure of the compact's shear strength. β is a measure of steepness of the shear failure line. p_b is the amount of stress required to compact a material hydrostatically. R controls the shape of the cap line, and thus the ratio of p to q required for densifying a compact. However, there are only three data points per DPC envelop. The fourth independent parameter to satisfy the requirement is the normality of plastic flow vector (associative flow rule) which is not shown in the plot [5,10,14]. The plastic strain co-ordinates are superimposed upon the in-die compaction stress co-ordinates on the yield cap surface. The plastic strain increment vector is outward, normal to the yield cap surface at the in-die stress co-ordinates.

3. Materials and Methods

3.1. Virgin MCC

MCC powder (Avicel PH200, FMC, PA, USA) was used as the starting material to produce monodisperse granules of four different SF which were forward processed into tablets. A 150 – 250-μm size fraction of MCC powder was obtained by sieving and was referred to as 200 μm V-MCC. V-MCC was equilibrated at 20°C/30% RH condition for 24 hours prior to forward processing to eliminate the impact of moisture content variability on the mechanical properties of the compact [15]. The true density of V-MCC was determined to be 1.556 g/cc by helium pycnometry, which is consistent with literature [12]. The SF of a tapped bed of V-MCC powder was determined to be 0.25 [12].

3.2. Monodisperse Granule Preparation

Monodisperse granules of precisely controlled size (1.5 mm diameter x 1.5 mm thickness), shape (biconvex cylindrical compact), and SF (nominally 0.42, 0.54, 0.60, and 0.69) were produced by directly compressing V-MCC powder using a Korsch EK0 (Korsch Pressen, Berlin, Germany) tablet press equipped with standard concave, multi-tip tooling. Monodisperse granules were equilibrated at 20°C/30% RH condition for at least 24 hours and stored in an airtight glass container to allow post compaction relaxation prior to characterizing for weight, thickness, and breaking force, and forward processing into tablets. Neither the V-MCC powder nor the monodisperse granules were lubricated.

3.3. Compression of Tablets

A list of tablets prepared from V-MCC powder and monodisperse granules is shown in Table 1. For each set of conditions, five tablets were made (n=5). Tablets were produced using an Instron universal testing machine (model 5569, Instron Ltd. Buckinghamshire, United Kingdom) equipped with 12-mm flat face tooling. Before compacting each tablet, the die wall and punch faces were lubricated with magnesium stearate powder. Compressive stresses of approximately 47, 83, and 159 MPa were used to produce tablets with nominal SF of 0.69,

0.79, and 0.89. The punch displacement rate was 5 mm/min for both compression and decompression phases. To allow post compaction relaxation, tablets were stored in airtight scintillation glass vials for at least 24 hours prior to testing for weight, thickness, and breaking force.

Table 1. Monodisperse Granules and Tablets Prepared There From

V-MCC Particle Size (μm)	Monodisperse Granules			Tablet		
	Diameter (mm)	Nominal Thickness (mm)	Nominal Solid Fraction	Nominal Solid Fraction	Nominal Thickness (mm)	Nominal Weight (mg)
200	1.5	1.5	0.42 0.54 0.60 0.69	0.69 0.79 0.89	6	745 850 955
					12	1485 1705 1905

3.4. Characterization

3.4.1. Solid Fraction of Monodisperse Granules and Tablets

Monodisperse granules and tablets were characterized out-of-die for weight, thickness, and breaking force. SF was calculated using Eq. 3 [16].

$$SF = \frac{(m/\rho)}{2 \cdot V_{cup} + A_{die}\ (t - 2 \cdot d_{cup})} \quad (3)$$

where m, ρ, V_{cup}, A_{die}, t *and* d_{cup} are defined as compact mass, true density of MCC, cup volume of the punch, die hole area, out-of-die thickness of the compact, and cup depth of the punch, respectively. V_{cup} and d_{cup} for flat face tablets were zero.

3.4.2. Diametrical Tensile Strength of Tablets

The diametrical breaking forces of 6 mm tall tablets were measured using an Instron universal testing machine (model 5569, Instron Ltd. Buckinghamshire, UK) at a compression rate of 5 mm/min.

Tablet TS (σ_{DC}) was calculated using equation below [17]:

$$\sigma_{DC} = \frac{2 \cdot F_c}{\pi \cdot D \cdot t} \quad (4)$$

where F_c, *and* D are defined as diametrical breaking force and diameter of the compact, respectively.

The hydrostatic stress (p_{DC}) and the deviatoric stress (q_{DC}) components of the tablet tensile stress state were obtained as [5]:

$$p_{DC} = \frac{2 \cdot \sigma_{DC}}{3} \quad (5)$$

$$q_{DC} = \sqrt{13} \cdot \sigma_{DC} \quad (6)$$

While equations 5 and 6 were utilized for consistency with Cunningham et al. and others in the literature [4,5,7,9,11], it should be noted that the stress state described by these equations is technically only applicable to the center of the tablet. Portions of the tablet closer to the compression platens are subjected to significantly larger stresses as described by Procopio et al. [18].

3.4.3. Uniaxial Compression Strength of Tablets

Uniaxial breaking forces of 12 mm tall tablets were measured using an Instron universal testing machine (model 5569, Instron Ltd. Buckinghamshire, UK). Tablets were compressed axially between two rigid platens at a compression rate of 5 mm/min. Ideally, the compact fails at a maximum shear stress developed at a 45° angle to the direction of applied axial stress [19,20]. Uniaxial compression strength of a tablet (σ_{UC}) was calculated using the relation below [5]:

$$\sigma_{UC} = \frac{4 \cdot F_{UC}}{\pi \cdot D^2} \quad (7)$$

where F_{UC} *is the* uniaxial breaking force of the tablet.

The hydrostatic stress (p_{UC}) and the deviatoric stress (q_{UC}) components of the uniaxial compression stress state were obtained as [5]:

$$p_{UC} = \frac{\sigma_{UC}}{3} \quad (8)$$

$$q_{UC} = \sigma_{UC} \tag{9}$$

3.4.4. In-die Compaction of Tablets - Axial and Radial Stresses and Elastic Properties

An Instron equipped with a 50 kN load cell, and an instrumented die with 12-mm round flat face punches, were used for in-die compaction of 12-mm tall tablets. A piezoelectric stress sensor (2.5 mm diameter, model 6159A- SN4257057, Kistler Instruments AG) was mounted in the die wall, ground cylindrically, and was in contact with the powder compact. The center of the sensor was positioned such that it collected the peak radial stress from the middle of the tablet. The compression and decompression rate was 5 mm/min with zero dwell time. Axial stress data were logged by the Instron data acquisition system. Radial stress data were logged using an Omega OM-SQ2040 data recorder equipped with a Kistler charge amplifier type 5073 - RS232c. Data logging frequency was 100 Hz throughout the compression and decompression processes. For each compaction cycle, the inner die wall and punch tips were lubricated with magnesium stearate powder prior to adding powder or granules into the die cavity.

The axial stress (σ_{ICA}) was calculated as [5]:

$$\sigma_{ICA} = \frac{4 \cdot F_{ICA}}{\pi \cdot D^2} \tag{10}$$

where F_{ICA} is the peak axial force. The peak radial stress (σ_{ICR}) was captured directly by the radial sensor without additional calculations.

The hydrostatic stress (p_{IC}) and the deviatoric stress (q_{IC}) components were also determined from the maximum axial and radial stresses recorded during the in-die compaction process [5].

$$p_{IC} = \frac{\sigma_{ICA} + 2 \cdot \sigma_{ICR}}{3} \tag{11}$$

$$q_{IC} = \sigma_{ICA} - \sigma_{ICR} \tag{12}$$

The axial strain (ε_A) was calculated as [5]:

$$\varepsilon_A = Ln[(H_0 - P_U + P_D)/H_0] \tag{13}$$

where H_0 is the initial specimen height, P_U is the upper punch displacement, and P_D is the punch deformation determined by compressing the punches in an empty die cavity.

From the slope of the decompression phase of the axial and radial stress versus axial strain profiles, Poisson's ratio (v) and Young's modulus (E) were calculated using Eqs. 14 and 15 [5]. A linear fit of the top 200 data points corresponding to the first two seconds of decompression was used to calculate slopes for all the samples. Assumptions are made that the radial strain is zero, and the circumferential and radial stresses are equal.

$$v = \frac{\left(\frac{d\sigma_{ICR}}{d\varepsilon_A^e}\right)}{\left(\frac{d\sigma_{ICR}}{d\varepsilon_A^e}\right) + \left(\frac{d\sigma_{ICA}}{d\varepsilon_A^e}\right)} \tag{14}$$

$$E = \left(\frac{d\sigma_{ICA}}{d\varepsilon_A^e}\right) - 2v\left(\frac{d\sigma_{ICR}}{d\varepsilon_A^e}\right) \tag{15}$$

where $\left(\frac{d\sigma_{ICA}}{d\varepsilon_A^e}\right)$ and $\left(\frac{d\sigma_{ICR}}{d\varepsilon_A^e}\right)$ are the slope of the decompression phase of the axial stress to elastic strain and the radial stress to elastic strain curve, respectively. ϵ_A^e is the elastic strain during the decompression phase.

3.4.5. Determination of DPC Parameters

DPC parameters were determined based on the work by Cunninghum et al. [5]. From the uniaxial compression and diametrical breaking force tests, material cohesion (d) was calculated using the following equation:

$$d = \frac{\sigma_{UC}\cdot\sigma_{DC}\cdot\left(\sqrt{13}-2\right)}{\sigma_{UC}+2\cdot\sigma_{DC}} \tag{16}$$

The internal friction angle (β) of the material was calculated using Eq. 17:

$$\beta = \tan^{-1}\left[\frac{3\cdot(\sigma_{UC}-d)}{\sigma_{UC}}\right] \tag{17}$$

The pressure evolution parameter (p_a) was calculated as:

$$p_a = \frac{-(3\cdot q_{IC}+4\cdot d\cdot\tan\beta)+\sqrt{(9\cdot q_{IC}^2+24\cdot d\cdot q_{IC}\cdot\tan\beta+24\cdot p_{IC}\cdot q_{IC}\cdot(\tan\beta)^2+16\cdot q_{IC}^2\cdot(\tan\beta)^2)}}{4\,(\tan\beta)^2} \tag{18}$$

The cap eccentricity parameter (R) was calculated using Eq.19:

$$R = \sqrt{\frac{2\cdot(p_{IC}-p_a)}{3\cdot q_{IC}}} \tag{19}$$

The hydrostatic yield stress (p_b) was calculated using the following equation:

$$p_b = p_a + R \cdot [d + p_a \cdot \tan\beta] \tag{20}$$

4. Results and Discussion

4.1. Tablets Produced from V-MCC and Monodisperse Granules

Figure 2 shows optical images of tablets prepared from V-MCC and monodisperse granules with initial solid fractions of 0.42, 0.54, 0.60, and 0.69 SF. Each tablet was compressed to the same average SF of 0.69.The top images show a top view of tablets and the bottom images show a side view of tablets. Despite having the same total porosity, there is a substantial variation in the tablet microstructure as a function of the initial granule SF. As the initial granule SF increased, tablet surfaces were rougher, with more defined granular structures remaining in the final tablet. This observation is consistent with the experimental results described in the literature [12,13].

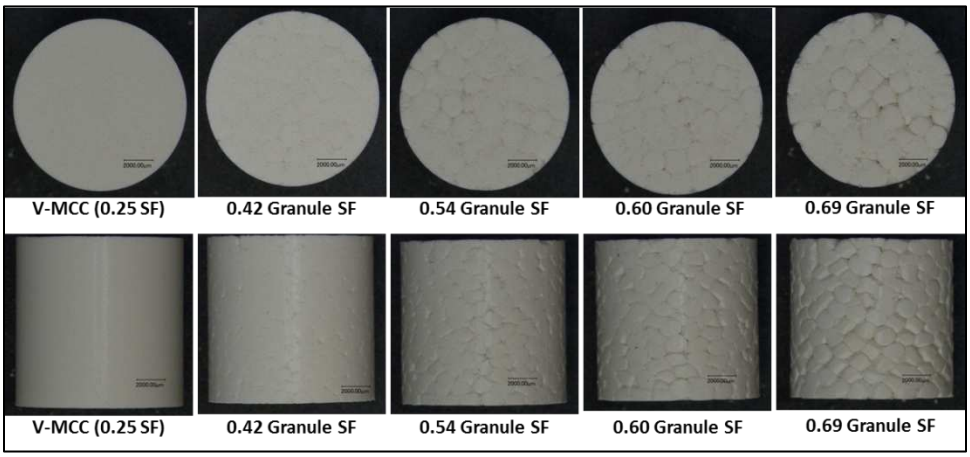

Figure 2. Optical Images of Flat Face Surfaces (top) and Cylindrical Surfaces (bottom) of 0.69 SF Tablets Prepared from V-MCC powder and 0.42, 0.54, 0.60, and 0.69 SF Monodisperse Granules.

The peak axial stress exerted by the upper punch and the peak radial stress exerted on the die wall during the confined compression process are plotted against initial granule SF in Figure 3 and Figure 4, respectively. Because MCC behaves as if self-lubricated [21], and the die wall and punch faces were lubricated, it is reasonable to assume that the upper punch force was completely transmitted through the tablet. Results show that SF of the initial powder/granules does not significantly impact the axial or radial stress at a given tablet SF. In other words, granulation apparently did not impact these measures of MCC densification behavior. In general, radial stresses were slightly more variable at higher initial granule SF, which could be attributed to the roughness of the cylindrical surface (Figure 2) and resultant variability of the number of granules in contact with the radial stress sensor. Radial stress increased as the axial stress increased. Radial stress only slightly increased as the initial granule SF increased. Irrespective of the granulation state, the radial stress was around 27%, 35%, and 45% of the axial stress for 0.69, 0.79, and 0.89 SF tablets, respectively.

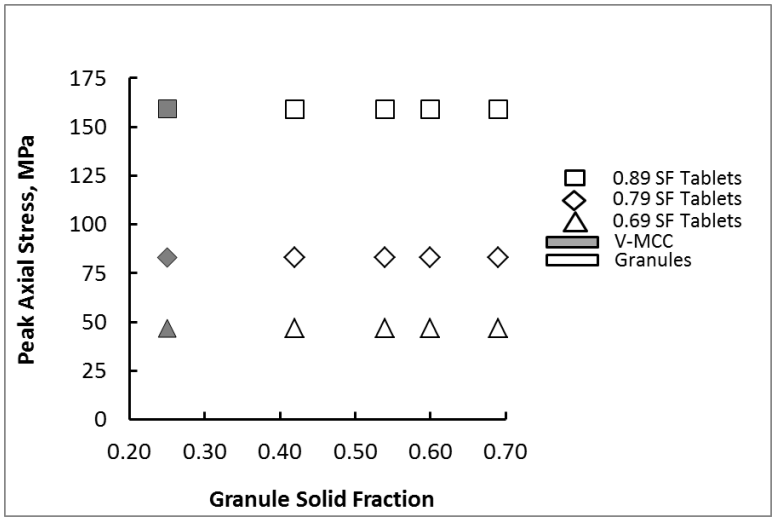

Figure 3. Axial Stresses versus Granule Solid Fraction. Triangle (Δ), diamond (◊) and Square (□) markers represent nominally 0.69, 0.79, and 0.89 SF tablets, respectively. Grey markers represent V-MCC and open markers represent monodisperse granules.

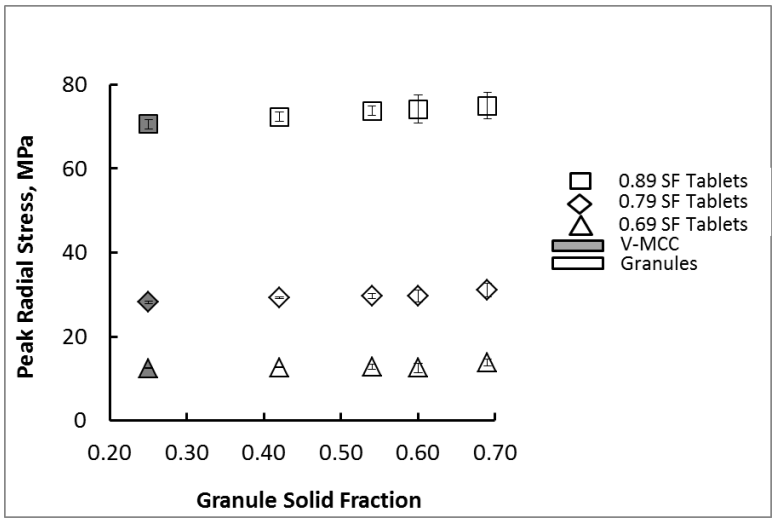

Figure 4. Radial Stresses versus Granule Solid Fraction. Triangle (Δ), diamond (◊) and Square (□) markers represent nominally 0.69, 0.79, and 0.89 SF tablets, respectively. Grey markers represent V-MCC and open markers represent monodisperse granules.

Diametrical TS of tablets of nominally 0.69, 0.79, and 0.89 SF are plotted against initial granule SF in Figure 5. Uniaxial compression strengths are shown in Figure 6. In both cases, strength increased with decreasing initial powder/granule SF. In other words, the fracture resistance of MCC depends strongly on initial granule SF [12,13]. At a given tablet SF, the strength decreased linearly as the granule SF increased. However, the slope of the linear fit was larger at a higher tablet SF. Overall, the diametrical TS was approximately 8% of the uniaxial compression strength with a clear trend of slightly lower ratio at a higher initial granule SF and higher tablet SF. This value is reasonably close to that reported for MCC (around 9%) in the literature [22].

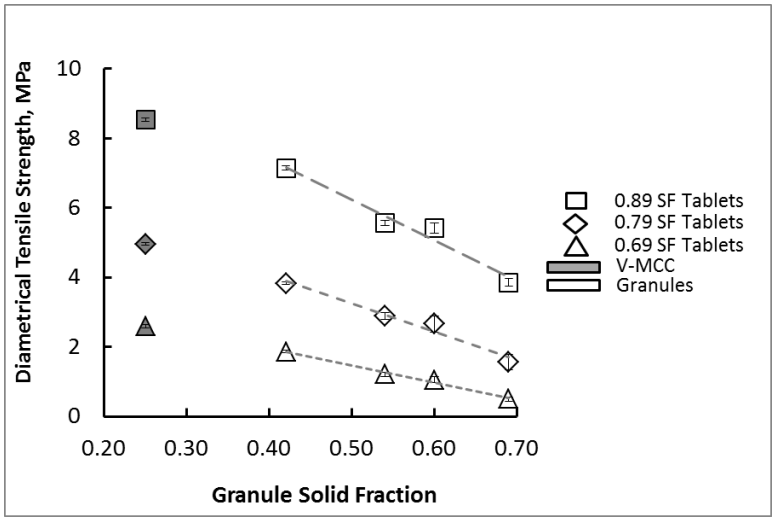

Figure 5. Diametrical Tensile Strength of Tablets (6 mm tall) versus Granule Solid Fraction. Triangle (Δ), diamond (◊) and Square (□) markers represent nominally 0.69, 0.79, and 0.89 SF tablets, respectively. Grey markers represent V-MCC, and open markers represent monodisperse granules. Dotted lines are the linear fits.

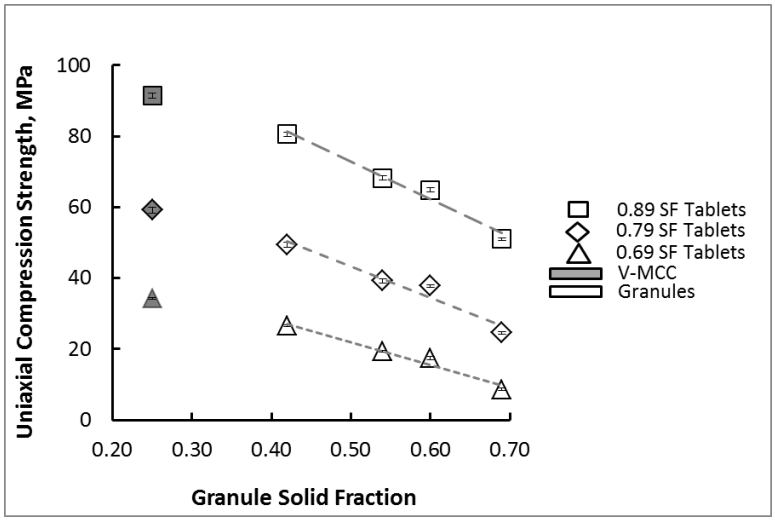

Figure 6. Uniaxial Compression Strength of Tablets (12 mm tall) versus Granule Solid Fraction. Triangle (Δ), diamond (◊) and Square (□) markers represent nominally 0.69, 0.79, and 0.89 SF tablets, respectively. Grey markers represent V-MCC, and open markers represent monodisperse granules. Dotted lines are the linear fits.

4.2. The DPC Model Parameters

In Figure 7, cohesion (*d*) is plotted against initial granule SF. *d* of V-MCC powder was around 5, 10, and 17 MPa when compressed to nominally 0.69, 0.79, and 0.89 SF tablets. *d* of MCC decreases with increasing initial granule SF. This is the expected trend since *d* is calculated directly from the diametrical compression and uniaxial compression test data (Figures 5 and 6). These values were similar to those reported by Swaminathan et al. [9**Error! Bookmark not defined.**].

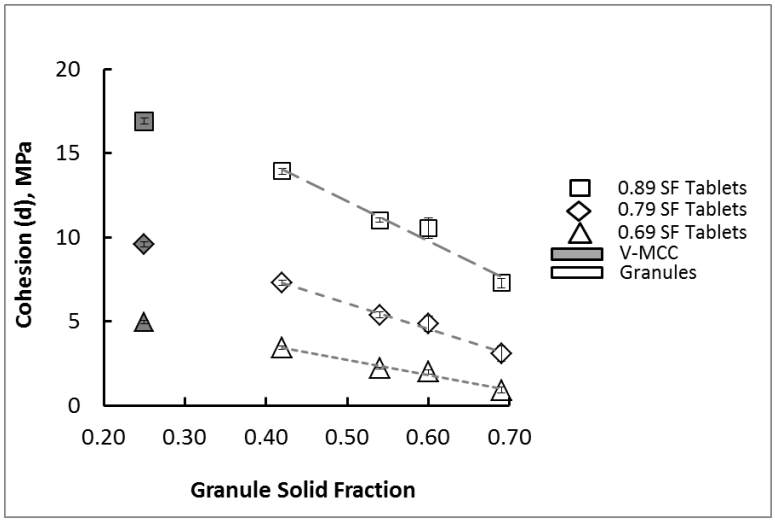

Figure 6.7. Cohesion versus Granule Solid Fraction. Triangle (Δ), diamond (◊) and Square (□) markers represent nominally 0.69, 0.79, and 0.89 SF tablets, respectively. Grey markers represent V-MCC, and open markers represent monodisperse granules. Dotted lines are the linear fits.

The internal angle of friction (β) of materials is plotted against initial granule SF in Figure 8. For brittle materials such as tablets, which are stronger (higher fracture resistance) under compression (higher hydrostatic stress, *p*) than under tension, β measures the sensitivity of the compression-induced strengthening. In this case, β was found to be insensitive to initial powder/granule SF as well as to final tablet SF. β only varied between 68° and 70° similar to values reported by Swaminathan et al. [9].

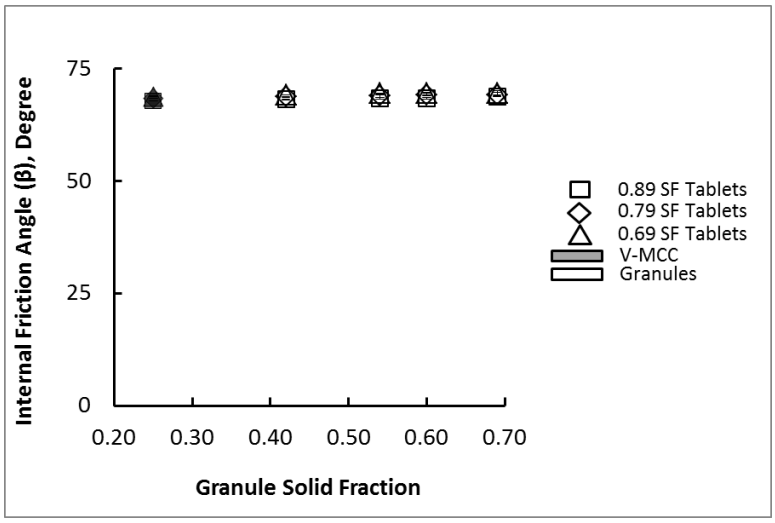

Figure 8. Internal Friction Angle versus Granule Solid Fraction. Triangle (Δ), diamond (◊) and Square (□) markers represent nominally 0.69, 0.79, and 0.89 SF tablets, respectively. Grey markers represent V-MCC, and open markers represent monodisperse granules.

In Figure 9, cap eccentricity parameter (*R*) is plotted against granule SF. *R* was not significantly impacted by granulation or granule SF. As the granule SF increased *R* decreased slightly at 0.69 tablet SF but increased slightly at 0.79 and 0.89 tablet SF. *R* was slightly more variable at higher granule SF. In contrast, at any given granule SF, *R* increased significantly as the tablet SF increased; the values were around 0.43, 0.53, and 0.67 for nominally 0.69, 0.79, and 0.89 SF tablets, respectively. These values are similar to those reported by Cunninghum et al. [5] and Sinka et al. [23].

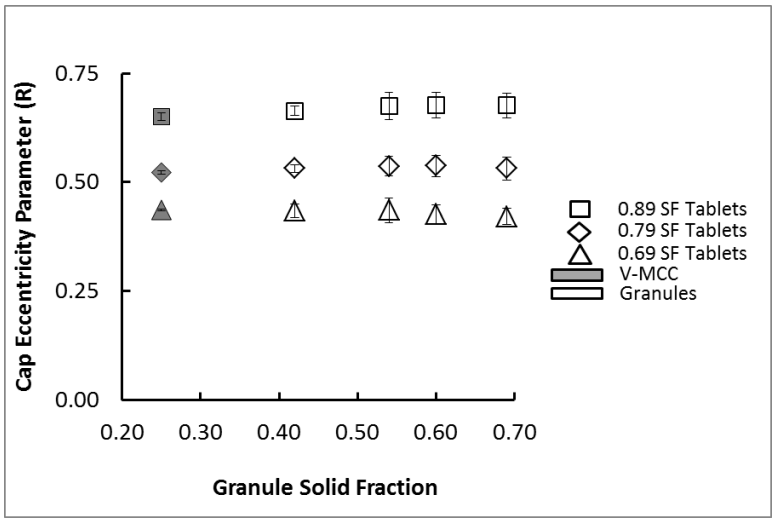

Figure 9. Cap Eccentricity Parameter versus Granule Solid Fraction. Triangle (Δ), diamond (◊) and Square (□) markers represent nominally 0.69, 0.79, and 0.89 SF tablets, respectively. Grey markers represent V-MCC, and open markers represent monodisperse granules.

Hydrostatic yield strength (P_b) of materials is plotted against granule SF in Figure 10. Similar to the cap eccentricity parameter, P_b increased significantly as the tablet SF increased, but was not significantly impacted by the dry granulation or granule SF. P_b was 32, 61, and 126 MPa for nominally 0.69, 0.79, and 0.89 SF tablets, respectively which are similar to those reported by Swaminathan et al. [9**Error! Bookmark not defined.**]. This is the expected trend since P_b is determined from the axial and radial stresses measured during in-die compression. P_b is a function of the densification behavior of powder in the die. The results indicate that all the materials, irrespective of granulation status, required the same amount of stress to densify to a specific tablet SF. Once the tablet SF reaches 1, the tablet would not densify any further even at a very high applied stress (fully dense material behavior) [5,10,23]. However, the compact could still fail by fracture.

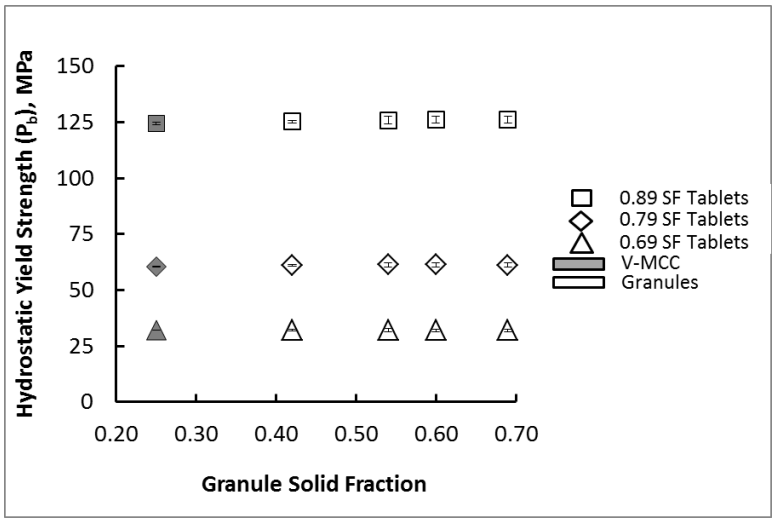

Figure 10. Hydrostatic Yield Strength versus Granule Solid Fraction. Triangle (Δ), diamond (◊) and Square (□) markers represent nominally 0.69, 0.79, and 0.89 SF tablets, respectively. Grey markers represent V-MCC, and open markers represent monodisperse granules.

The DPC model-fitting curves (represented by solid and dotted lines) for 0.69, 0.79, and 0.89 SF tablets prepared from V-MCC and 0.42, 0.54, 0.60, and 0.69 SF monodisperse granules are shown in *p-q* plane in Figure 11. Hydrostatic stress and deviatoric stress components of the diametrical tensile stress (open markers), uniaxial compression stress (grey markers), and in-die compaction stress state (black markers) are also shown. The triangle (Δ), diamond (◊) and square (□) symbols represent 0.69, 0.79 and 0.89 SF tablets, respectively.

In the insert, the plot clearly shows the cohesion of materials, the only parameter that was significantly impacted by the dry granulation and the granule SF. The cohesion was higher for V-MCC, and it decreased as the granule SF increased or the tablet SF decreased. The yield cap curves for all the materials were comparable and depended on the tablet SF, but not the initial powder/granule SF. The DPC parameters predicted that while V-MCC and granules required the same amount of stress to densify to a given tablet SF, V-MCC and lower SF granules would produce compacts that could withstand higher stress before fracture. The in-die compaction stress path (*p,q* coordinate of the maximum in-die compaction stress in the *p-q* plane) of all the materials was similar at a given tablet SF. However, at higher tablet SF, the position of the in-die compaction stress point on the yield

cap shifted away from the shear failure line [23]. Magnitude of the hydrostatic stress component of the in-die compaction stress state increased relative to the deviatoric stress component as the tablet SF increased; the *p*-to-*q* ratio was 0.77, 0.91, and 1.11 at tablet SF of 0.69, 0.79, and 0.89, respectively. This suggests that as the tablet SF increases, the stress state becomes more hydrostatic.

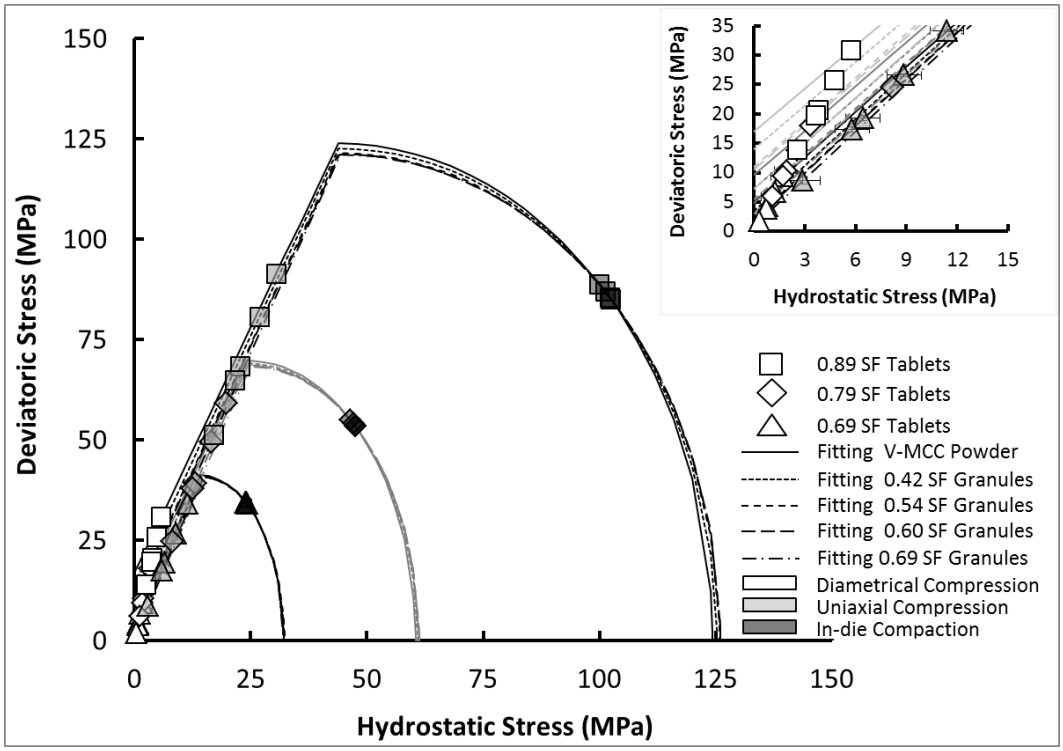

Figure 11. DPC Profiles for V-MCC and Monodisperse Granules. Triangle (Δ), diamond (◊) and Square (□) markers represent experimental data points for nominally 0.69, 0.79, and 0.89 SF tablets, respectively. Solid and dotted lines are model fitting curves for the materials.

In Figures 12 and 13, Poisson's ratio (υ) and Young's modulus (E), respectively, are plotted against initial granule SF. As seen for most of the DPC parameters, υ and E were independent of initial powder/granule SF. This suggests that at a given tablet SF, all the materials will produce tablets with similar stiffness which will have similar post compaction recovery during the unloading and ejection step. In contrast, at any given granule SF, both υ and E increased as the tablet SF increased. υ was approximately 0.09, 0.12, and 0.17 and E was approximately 4, 10, and 17 GPa for 0.69, 0.79, and 0.89 SF tablets, respectively, which

are close to the values reported by Swaminathan et al. [9]. Higher SF tablets are expected to have higher ejection stress but smaller post compaction recovery during the unloading and ejection steps. A compact with low E and high υ value typically poses risk of formation of hairline crack or lamination during the ejection process [11]. In the literature the value of υ for MCC varied widely; it was reported 0.12-0.25 for nominally 0.7 SF tablets, and 0.28-0.35 for nominally 0.9 SF tablet [5,9,11,23]. Similar variation of E is also reported by the same authors - ~3-10 GPa for nominally 0.7 SF tablets and ~5-28 GPa for 0.9 SF tablets. One factor that could cause this variability is the portion of decompression curve used to calculate υ and E [23]. Other potential factors could be the inconsistency in correcting the axial strain for machine/tooling stiffness [5]. In our study, axial strain was corrected for punch deformation (Eq. 13).

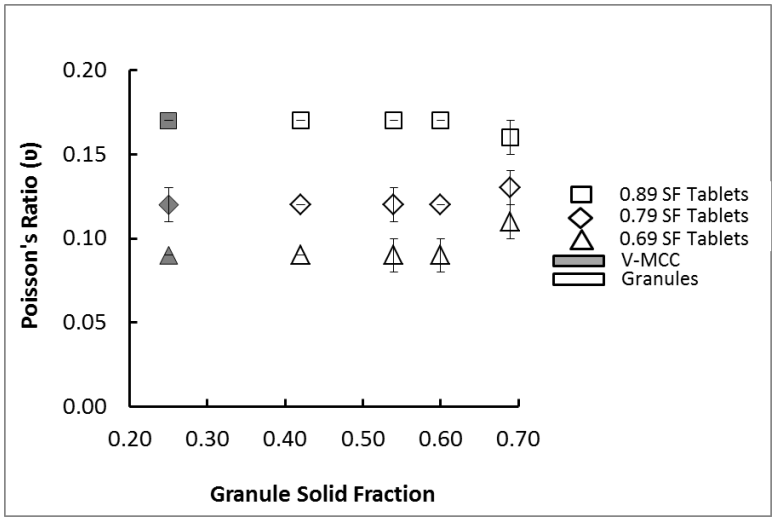

Figure 12. Poisson's Ratio versus Granule Solid Fraction. Triangle (Δ), diamond (◊) and Square (□) markers represent nominally 0.69, 0.79, and 0.89 SF tablets, respectively. Grey markers represent V-MCC and open markers represent monodisperse granules.

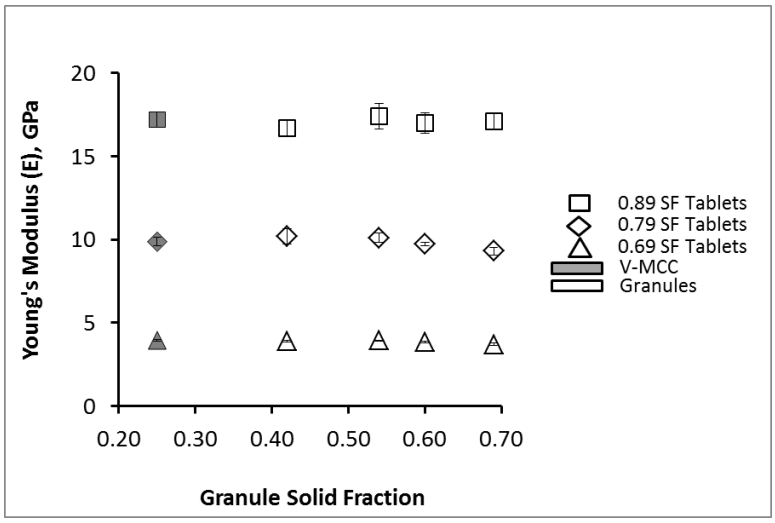

Figure 13. Young's Modulus versus Granule Solid Fraction. Triangle (Δ), diamond (◊) and Square (□) markers represent nominally 0.69, 0.79, and 0.89 SF tablets, respectively. Grey markers represent V-MCC and open markers represent monodisperse granules.

5. Discussion

The experimental results in this study show that despite the difference in stress history, both V-MCC and monodisperse granules require the same in-die compaction stress state (comparable p, q co-ordinates) to achieve a certain tablet SF. However, as the tablet SF increases, the ration of the hydrostatic stress component to the deviatoric stress component becomes larger. It should be noted that a high SF granule bed would only undergo a small increase in SF to achieve the final tablet SF, compared to a low SF granule bed [13]. The tablet matrices from high SF granules would contain more void spaces between the neighboring granules, undergo more extra-granular failure during diametrical compression testing and exhibit low tensile strength.

Dry granulation decreases the cohesion--that is, the shear strength of tablets from high SF granules versus V-MCC and the tablets produced from higher SF granules are weaker. Tablets prepared from V-MCC or any granule states have comparable elastic modulus and

Poisson's ratio therefore would exhibit similar stiffness and undergo similar post compaction recovery during the unloading and ejection processes. However, higher SF tablets would experience less post compaction recovery but higher ejection stress.

This study clearly shows that dry granulation of V-MCC and stress history of granules (granule SF) mainly impact one of the DPC parameters: cohesion. Therefore, complete experimental calibration of all the DPC parameters may not be necessary for both V-MCC and MCC granules. Once the model is completely calibrated for V-MCC, only calibration of the shear failure surface for granules may be adequate. This will require only two experimental data sets: diametrical tensile strength and uniaxial compression strength of tablets. This approach, by eliminating the in-die compaction test, will significantly reduce the experimental burden to study compaction behavior of granules using the DPC model.

6. Conclusions

Calibration of the Drucker Prager Cap (DPC) model parameters provided a means for a deeper understanding of the impact of dry granulation and granule SF on the compaction behavior of plastically deformable systems. Despite the granulation status, all the materials required the same amount of pressure to produce tablets of a given SF. However, as the tablet SF increased, the ratio of the hydrostatic to deviatoric stress component of the in-die compaction stress path increased. Dry granulation and increased SF of granules decreased the cohesion of the material and TS of the tablets. All other parameters including the *p, q* co-ordinate of the in-die compaction stress state, Young's modulus, and Poisson's ratio were only impacted by the tablet SF. Material behaviors such as compressibility, ejection stress, and post compaction recovery during the unloading and ejection steps would not be impacted by the dry granulation of MCC. Since, cohesion is the only impacted parameter, calibration only of the shear failure surface would be sufficient to understand the compaction behavior of MCC granules when a full calibration for V-MCC is available.

References

[1] C. K. Tye, C. Sun, G. E. Amidon, 2005, Evaluation of the effects of tableting speed on the relationships between compaction pressure, tablet tensile strength, and tablet solid fraction, J. Pharm. Sci. 94, 465-472

[2] I. Akseli, N. Ladyzhynsky, J. Katz, X. He, 2013, Development of predictive tools to assess capping tendency of tablet formulations. Powder Technol 236:139–148

[3] G. Alderborn, C. Nystrom, Pharmaceutical Powder Compaction Technology, vol 71, Pharmacy, Marcel Dekker, New York, 1996

[4] I. C. Sinka, 2007, Modelling Powder Compaction, KONA, 25, 4-25

[5] J. Cunningham, I.C. Sinka, A. Zavalingos, 2004, Analysis of tablet compaction. I. Characterization of mechanical behavior of powder and powder/tooling friction. J Pharm Sci. 93 (8): 2022-2039

[6] A. Michrafy, D. Ringenbacher, P. Tchoreloff, 2002. Modelling the compaction behavior of powders: application to pharmaceutical powders. Powder Technology. 127: 257-266

[7] L.H. Han, J.A. Elliott, A.C. Bentham, A. Mills, G.E. Amidon, B.C. Hancock, 2008. A modified Drucker-Prager Cap model for die compaction simulation of pharmaceutical powders. Int. J. Solids and Structures 45: 3088-3106

[8] A. R. Muliadi, J. D. Litster, C. R Waasgren, 2013, Validation of 3-D finite element analysis for predicting the density distribution of roll compacted pharmaceutical powder, Powder Technology, 237, 386-399

[9] S. Swaminathan, A. R. Muliadi, P. Geldenhuis, S. Yuk, C. R. Wassgren, J. D. Litster, The modified Drucker-Prager/Cap properies of pharmaceutical powders, AIChE annual meeting, 2012, Pittsburgh, PA

[10] H. Diarra, V. Mazel, A. Boillon, L. Rehault, V. Busignies, S. Bureau, P. Tchoreloff, 2012, Finite element method (FEM) modeling of the powder compaction of cosmetic products: comparison between simulated and experimental results, Powder Technology, 224, 233-240

[11] K. LaMarche, D. Buckley, R. Hartley, F. Qian, S. Badawy, 2014, Assessing materials' tablet compaction properties using the Drucker-Prager Cap model, Powder Technology, 267, 208-220

[12] B. Mitra, J. Hilden, J. D. Litster, 2015, Novel use of monodisperse granules to deconvolute impacts of granule size versus granule solid fraction on tablet tensile strength, Advanced Powder Technology, 26 (2015) 553-562

[13] B. Mitra, J. Hilden, J. D. Litster, 2015, color gran paper

[14] W. F. Chen, D. J. Han Stress strain relations for perfectly plastic materials, In: Plasticity for Structural Engineers, 2007, J Ross Publishing, Fort Lauderdale, FL

[15] C. Sun, Mechanism of moisture induced variations in true density and compaction properties of microcrystalline cellulose, International Journal of Pharmaceutics, 346 (2008) 93-101

[16] J. Hilden, G. Earle, 2011, Prediction of roll compacted ribbon solid fraction for quality by design development, Powder Technology, 213, 1–13.

[17] J. T. Fell, J. M. Newton, 1970, Determination of tablet strength by the diametrical compression test, J. Pharm. Sci., 59(5), 688-691

[18] A. Procopio, A. Zavaliangos, J. Cunningham, 2003, Analysis of the diametrical compression test and the applicability tp plastically deforming materials, J. Mat. Sci. 38, 3629 – 3639

[19] E. I. Al-Sahawneh, 2013, Size effect and strength correction factors for normal weight concrete specimens under uniaxial compression stress, Contemporary Engineering Sciences, 6(2), 57 – 68

[20] B. Johnston, D. Mazurek, Mechanics of Materials, 6th edition (global edition), 2012, McGraw Hill, New York.

[21] M. T. Decrosta, J. B. Schwartz, R. J. Wigent, K. Marshall, 2001, Thermodynamic analysisof compact formation; compaction, unloading, and ejection: II. Mechanical energy (work) and thermal energy (heat) determinations of compact unloading and ejection, Int. J. Pharm., 213, 45-62

[22] J. M. Newton, G. Alderborn, C. Nystrom, P. Stanley, 1993, The compressive to tensile strength ratio of pharmaceutical compacts, Int. J. Pharm., 93, 249-251

[23] I.C. Sinka, J. Cunningham, A. Zavalingos, 2003. The effect of wall friction in the compaction of pharmaceutical tablets with curved faces: a validation study of the Drucker-Prager Cap model. Powder Technol, 133: 33-43